AN ELEMENT-BASED FINITE-VOLUME METHOD APPROACH FOR NATURALLY FRACTURED COMPOSITIONAL RESERVOIR SIMULATION

Francisco Marcondes, marcondes@ufc.br
Federal University of Ceará - Department of Metallurgical Engineering and Material Science

Abdoljalil Varavei, varavei@mail.utexas.edu
The University of Texas at Austin – Petroleum and Geosystems Engineering Department

Kamy Sepehrnoori, kamys@mail.utexas.edu
The University of Texas at Austin – Petroleum and Geosystems Engineering Department

Abstract. *An element-based finite-volume approach in conjunction with unstructured grids for naturally fractured compositional reservoir simulation is presented. In this approach, both the discrete fracture and the matrix mass balances are taken into account without any additional models to couple the matrix and discrete fractures. The mesh, for two dimensional domains, can be built of triangles, quadrilaterals, or a mix of these elements. However, due to the available mesh generator to handle both matrix and discrete fractures, only results using triangular elements will be presented. The discrete fractures are located along the edges of each element. To obtain the approximated matrix equation, each element is divided into three sub-elements and then the mass balance equations for each component are integrated along each interface of the sub-elements. The finite-volume conservation equations are assembled from the contribution of all the elements that share a vertex, creating a cell vertex approach. The discrete fracture equations are discretized only along the edges of each element and then summed up with the matrix equations in order to obtain a conservative equation for both matrix and discrete fractures. In order to mimic real field simulations, the capillary pressure is included in both matrix and discrete fracture media. In the implemented model, the saturation field in the matrix and discrete fractures can be different, but the potential of each phase in the matrix and discrete fracture interface needs to be the same. The results for several naturally fractured reservoirs are presented to demonstrate the applicability of the method.*

Keywords*: Naturally fractured reservoirs, Discrete fractured model, Compositional reservoir simulation, EbFVM.*

1. Introduction

Naturally fractured reservoirs play an important role in petroleum reservoir simulations since a large amount of oil and gas around the world are stored inside these types of reservoirs. According to Monteagudo and Firoozabadi (2004), about 20 percent of all the oil and gas production around the world is produced from naturally fractured reservoirs. Several approaches have been proposed to model the fluid flow in the naturally fractured reservoirs, such as the dual porosity model (Warren and Roog, 1963; Odeh, 1965; Kazemi, 1969; Kasemini et *al.*, 1976, Reza et *al.*, 2007). In the dual porosity model, the reservoir is divided in blocks also known as sugar cubes. The region inside each block represents the matrix, a region of highly stored capacity but of low permeability. The region surrounding each block represents the discrete fractures, which have higher permeability values than the matrix region. A transfer function is necessary in order for these two regions to communicate as there is no communication between matrix blocks. Another approach commonly used is the dual porosity/dual permeability model (Lingen et *al.*, 2001; Magras et. *al.*, 2001; Al-Huthali and Datta-Grupta, 2004). In this method, there is communication between the matrix blocks and fractures. The drawback of the mentioned above methods is the representation of complex discrete fracture configurations. One method that can accommodate most of the features of complex fracture configurations is the discrete fractured model (Noorishad and Mehrn, 1982; Monteagudo and Firoozabadi, 2004; Baca et *al.*, 2005). In this method, as discussed by Monteagudo and Firozabadi (2004), the conservation equations for both matrix and discrete fractures are summed up in order to obtain a final equation for both media.

In this paper, we used an approach similar to the one used by Monteagudo and Firoozabi (2004) to model the compositional fluid flow in naturally fractured reservoirs. The discrete fractured model was implemented in an in-house compositional simulator called GPAS (General Purpose Adaptive Simulator). GPAS was developed at the Center for Petroleum and Geosystems Engineering at The University of Texas at Austin for the simulation of enhanced recovery processes. GPAS is a fully implicit, multiphase/multi-component simulator which can handle the simulation of several enhanced oil recovery processes. The approximate equations for the matrix are obtained through the EbFVM –Element based Finite-Volume Method (Cordazzo, 2004; Cordazzo, et *al.*, 2004a-b; Marcondes and Sepehrnoori, 2007; Marcondes and Sepehrnoori, 2010). For 2D reservoirs, the discrete fractures are located along the edges of the elements as shown in Fig. 1. In this approach, we just apply the classical control-volume method to obtain the approximate equations for the discrete fractures. In order to mimic real field simulations, the capillary pressure is included in both

matrix and discrete fracture potentials. In the implemented model, the saturation field in the matrix and the discrete fracture can be different, but the potential of each phase in the interface of the matrix and the discrete fracture needs to be the same. The results for several naturally fractured reservoirs are presented to demonstrate the applicability of the method.

2. Physical Model

Isothermal, multi-component, multiphase fluid flow in a porous medium can be described using three types of equations: the component-material balance equation, the phase equilibrium equation, and the equation for constraining phase saturations and component concentrations (Wang *et al.*, 1997).

The material balance equation for the *i-th* component for a full symmetric permeability tensor using the Einstein notation can be written as

$$\frac{\partial(\phi N_i)}{\partial t} - \nabla\bullet\left[\sum_{j=1}^{n_p}\xi_j\, x_{ij}\, \lambda_j \overline{\overline{K}}\bullet\nabla\Phi_j\right] - \frac{q_i}{V_b} = 0\ ;\ i=1,2,..,n_c. \tag{1}$$

In Equation (1), n_c is the number of hydrocarbon components, n_p is the number of phases present in the reservoir, ϕ is the porosity, N_i is the moles of the *i-th* component per unit of pore volume, ξ_j and λ_j are the molar density and relative mobility of the *j-th* phase, respectively, x_{ij} is the molar fraction of the *i-th* component in the *j-th* phase, $\overline{\overline{K}}$ is the absolute permeability tensor, and V_b is the volume of control-volume that has a well. Φ_j is the potential of the *j-th* phase and is given by

$$\Phi_j = P_j - \gamma_j Z, \tag{2}$$

where P_j denotes the pressure of the *j-th* phase and Z is depth, which is positive in a downward direction.

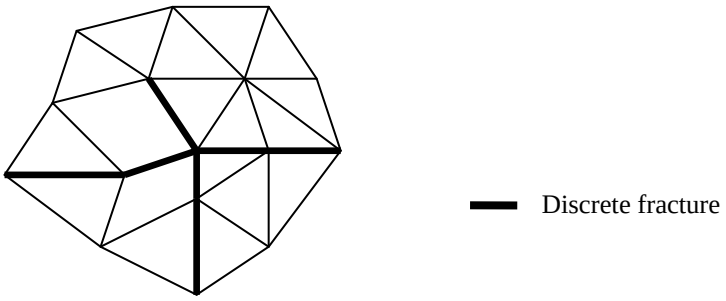

Figure 1. Zoom of the reservoir mesh with two discrete fractures included.

The first partial derivative of the total Gibbs free energy, with respect to the independent variables, gives the equality of component fugacities among all phases,

$$f_i = f_i^{\,j} - f_i^{\,r} = 0\ \ ;\ \ i=1,....,n_c\ \ \ ;\ \ j=2,.....,n_p. \tag{3}$$

In Equation (3), $f_i^{\,j} = \ln\left(x_{ij}\,\phi_{ij}\right)$, where ϕ_{ij} is the fugacity coefficient of component *i* in the *j-th* phase, *r* denotes the reference phase, and n_c is the number of components, excluding the water component. The restriction of the molar fraction is used to obtain the solution of Eq. (3),

$$\sum_{i=1}^{n_c} x_{ij} - 1 = 0\ ,\ j=2,..,n_p\ \ ;\ \ \sum_{i=1}^{n_c}\frac{z_i(K_i-1)}{1+\nu(K_i-1)} = 0, \tag{4}$$

where z_i is the overall molar fraction of the *i-th* component, K_i is the equilibrium ratio for the *i-th* component, and ν is the mole fraction of the gas phase in the absence of water. The closure equation comes from the volume constraint, *i.e*, the available pore volume of each cell must be filled by all phases present in the reservoir. This constraint gives rise to the following equation:

$$V_b\sum_{i=1}^{n_c+1}(\phi N_i)\sum_{j=1}^{n_p} L_j\,\overline{v}_j - V_p = 0, \tag{5}$$

where V_b is the bulk volume, V_p is the pore volume, and $\bar{v}_j$ is the molar volume of the *j-th* phase. Equation (1) is conservation equation for the matrix media. A similar conservation equation for the discrete fracture media is written as

$$\frac{\partial(\phi N_i)_f}{\partial t} - \nabla\bullet\left[\sum_{j=1}^{n_p}\xi_j\, x_{ij}\,\lambda_j \overline{\overline{K}}\bullet\nabla\Phi_j\right]_f - \frac{q_{if}}{V_{bf}} = 0\ ;\ i=1,2,..,n_c, \tag{6}$$

where the subscript *f* denotes discrete fracture media.

Using the continuity of capillary pressure at the interface of the matrix and the discrete fracture, we can evaluate the saturation field in the discrete fracture as a function of the saturation field in matrix media. As shown in Monteagudo and Firoozabi (2004), the saturation in the discrete fracture is given by

$$S_{wf} = (P_{c,f})^{-1} P_{c,m}(S_w), \tag{7}$$

where P_c denotes the capillary pressure for the oil-water system, and the subscript *m* denotes the matrix media. Equation (6) can be rewritten in terms of N_i using the chain rule and using Eq. (7) to evaluate the derivative of N_i with relation to S_w as

$$\frac{\partial N_{if}}{\partial N_i}\frac{\partial(\phi N_i)}{\partial t} - \nabla\bullet\left[\sum_{j=1}^{n_p}\xi_j\, x_{ij}\,\lambda_j \overline{\overline{K}}\bullet\nabla\Phi_j\right]_f - \frac{q_{if}}{V_{bf}} = 0\ ;\ i=1,2,..,n_c. \tag{8}$$

In GPAS, the unknown primary variables are water pressure P_w, N_1,..,N_{nc}, $\ln K_1$,.., $\ln K_{nc}$.

3. Aproximate Equations

In the EbFVM, each element is divided into sub-elements. These sub-elements will be called sub-control volumes. The conservation equation, Eq. (1), needs to be integrated for each sub-control volume. Figure 2 presents a triangular element and all of the sub-control volumes associated with each element. By integrating Eq. (1) in time and for each one of the sub-control volumes, and applying the Gauss theorem for the advective term, we obtain:

$$\int_V \frac{\partial(\phi N_i)}{\partial t} dV dt - \int_A \sum_{j=1}^{n_p}\xi_j\, x_{ij}\,\lambda_j \overline{\overline{K}}\bullet\nabla\Phi_j \bullet \overrightarrow{dA}\, dt - \int_V \frac{q_i}{V_b} dV\, dt = 0\ ;\ i=1,2,..,n_c, \tag{9}$$

To evaluate the first and second terms of Eq. (9), it is necessary to define the shape functions. The linear shape functions as defined by Eqs. (10) will be used.

$$N_1(s,t)=1-s-t\ \ ;\ \ N_2(s,t)=s\ \ ;\ \ N_3(s,t)=t. \tag{10}$$

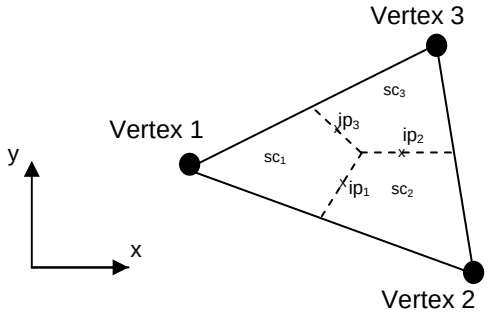

Figure 2. Triangular element and its respective sub-control volumes.

Using the shape functions, any physical properties or positions can be evaluated inside an element as

$$x(s,t)=\sum_{i=1}^{Nv} N_i\, x_i\ \ ;\ \ y(s,t)=\sum_{i=1}^{Nv} N_i\, y_i\ \ ;\ \ \Phi_j(s,t)=\sum_{i=1}^{Nv} N_i\,\Phi_{ji}, \tag{11}$$

where N_v denotes the number of vertex for each element. Using the shape functions, gradients of potentials can be easily evaluated as

$$\frac{\partial \Phi_j}{\partial x} = \sum_{i=1}^{Nv} \frac{\partial N_i}{\partial x} \Phi_{ji} \quad ; \quad \frac{\partial \Phi_j}{\partial y} = \sum_{i=1}^{Nv} \frac{\partial N_i}{\partial y} \Phi_{ji}. \tag{12}$$

To evaluate the gradients, it is necessary to obtain the derivatives of shape functions relative to *x* and *y*. These derivatives are given by

$$\frac{\partial N_i}{\partial x} = \frac{1}{\det(J_t)} \left(\frac{\partial N_i}{\partial s} \frac{\partial y}{\partial t} - \frac{\partial N_i}{\partial t} \frac{\partial y}{\partial s} \right) \quad ; \quad \frac{\partial N_i}{\partial y} = \frac{1}{\det(J_t)} \left(\frac{\partial N_i}{\partial t} \frac{\partial x}{\partial s} - \frac{\partial N_i}{\partial s} \frac{\partial x}{\partial t} \right), \tag{13}$$

where J_t is the Jacobian of the transformation, given by

$$\det(J_t) = \left(\frac{\partial x}{\partial s} \frac{\partial y}{\partial t} - \frac{\partial x}{\partial t} \frac{\partial y}{\partial s} \right). \tag{14}$$

To perform the integration of Eq. (9), it is necessary to define the volumes of each sub-control volume and the area of each interface. The volumes of each sub-control is given by

$$Vscv_i = \frac{\det(J_t)\, \Delta s\, \Delta t\, h}{6}, \tag{15}$$

where *h* is the thickness of the reservoir. The area of each interface, reading a counterclockwise, is given by

$$\overrightarrow{dA} = h\, dy\, \vec{i} - h\, dx\, \vec{j}. \tag{16}$$

By substituting Eqs. (15) and (16) into Eq. (9), for the accumulation term and the advective flux term, respectively, and evaluating the fluid properties through a fully implicit procedure, the following equations for the two mentioned terms are obtained:

$$Acc_{m,i} = Vscv_{m,i} \left(\left(\frac{\phi N_m}{\Delta t} \right)_i - \left(\frac{\phi N_m}{\Delta t} \right)_i^o \right) \quad ; \quad m = 1, N_v, \tag{17}$$

$$F_{m,i} = \int_A \sum_{j=1}^{n_p} \xi_j\, x_{ij}\, \lambda_j \overline{\overline{K}} \bullet \nabla \Phi_j \bullet \overrightarrow{dA} = \int_A \sum_{j=1}^{n_p} \xi_j\, x_{ij}\, \lambda_j K_{np} \frac{\partial \Phi_j}{\partial x_p} dA_n \quad ; \quad m = 1, N_v \; ; \; n, p = 1, 2, \tag{18}$$

where the subscript *o* denotes properties evaluated in the previous time-step. By inspecting Eq. (17), it can be inferred that it is necessary to evaluate molar densities, molar fraction, and mobilities in two interfaces of each sub-control volume. To evaluate these properties, an upwind scheme based on Cordazzo *et al.* (2004a) will be used. For instance, the mobilities and other fluid properties are evaluated at the integration point 1 in Fig. 2 by

$$\begin{aligned} &\lambda_{j1} = \lambda_{j2} \quad if \quad \overline{\overline{K}}.\nabla \Phi_j.\overrightarrow{dA}\Big|_{ip1} \le 0 \\ &\lambda_{j1} = \lambda_{j1} \quad if \quad \overline{\overline{K}}.\nabla \Phi_j.\overrightarrow{dA}\Big|_{ip1} > 0. \end{aligned} \tag{19}$$

Inserting Eqs. (16) and (17) into Eq. (6), the following equation for each element is obtained:

$$Acc_{m,i} + F_{m,i} + q_i = 0 \quad ; \quad m = 1, N_v \; ; \; i = 1, n_c + 1. \tag{20}$$

Equation (20) denotes the conservation for each sub-control volume of each element. Now, it is necessary to assemble the equation of each control volume to ascertain the contribution of each sub-control volume sharing the same vertex. This process is similar to assembling the stiffness global matrix in the finite element method.

4. Test Problems

This section presents three simulation case studies using the EbFVM approach. The first two case studies were used to validate the present formulation with the results presented by Firoozabadi and Monteagudo (2004). The third case study presents a generic reservoir with six discrete fractures. Figure 3 presents the two-grid configurations used for case 1 and case 2 as well the discrete fracture configurations used for each case study. Table 1 presents the fluid and physical properties used for case studies 1 and 2. The Corey's relative permeability model was used for all case studies as given in Table 2, for both matrix (m) and discrete fractures (f). For case study 1, the discrete fracture is represented by a single line whose end point coordinates are: (0.2, 0.2) m and (0.8, 0.8) m. Table 3 presents the line coordinates used for case study 2. The general view of reservoirs used for case study 3 along with the discrete fracture configuration is presented in Fig. 4. For this case study, we have two injectors and two producers. We injected 2.3148×10^{-6} m^3/s of water into each well. The reservoir area was equal to 4,480.81 m^2 and reservoir thickness was equal to 3.048 m. The other physical parameters for this case are given in Table 1.

Table 1. Input data for case studies 1 and 2.

Reservoir data	Initial conditions	Physical properties and well conditions
Reservoir dimension ($L_x = L_y = L_z$ = 1 m Matrix: Absolute permeability: ($K_{xx}= K_{yy}$) = 9.87×10^{-16} m^2 (1 mD) Porosity = 0.2 Discrete Fracture: (K) = 8.26119×10^{-10} m^2 (837,000 mD) Porosity: 1.0 Width: 10^{-4} m	Water saturation S_{wi} = 0.0001 Reservoir pressure = 3.45 MPa (500 psi)	Water viscosity = 0.8×10^{-3} Pa.s Oil viscosity = 0.45×10^{-3} Pa.s Water injection rate = 2.3148×10^{-8} m^3/s Bottom hole pressure = 3.45 MPa (500psi)

Table 2. Corey's relative permeability model data

	Matrix (m)		Discrete fracture (f)	
	Water	Oil	Water	Oil
End point relative permeability	1.0	1.0	1.0	1.0
Residual saturation	0.2	0.1	0.0	0.0
Exponent of relative permeability	5.0	5.0	3.0	3.0

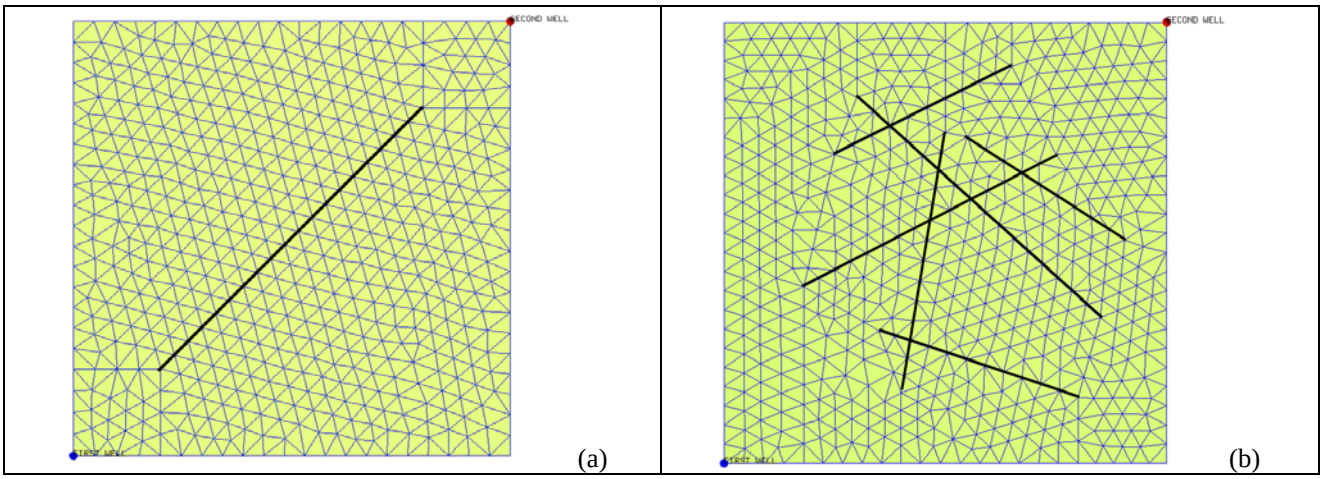

Figure 3. Mesh and discrete fracture configurations. a) Case study 1. b) Case study 2.

The capillary pressure used in this work is the same as the one used by Monteagudo and Firoozabadi (2004), given by

$$Pc(S_w) = -B_i \ln(S_w), \tag{20}$$

where *i* denotes the matrix (m) or discrete fracture (f) media. The unit used for Pc is in Pa.

Table 3. Fracture coordinates for case study 2.

Fractures	Coordinate of pont 1 (m)	Coordinate of point 2 (m)
1	(0.18, 0.40)	(0.75, 0.70)
2	(0.30, 0.83)	(0.85, 0.33)
3	(0.55, 0.74)	(0.87, 0.53)
4	(0.50, 0.75)	(0.40, 0.16)
5	(0.25, 0.70)	(0.65, 0.90)
6	(0.35, 0.30)	(0.80, 0.15)

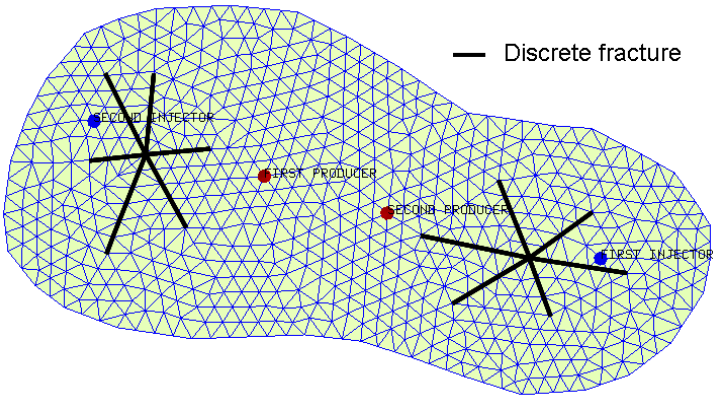

Figure 4. General reservoir with six discrete fractures.

5. Results

Figure 5 presents the results for case study 1, in terms of cumulative water and oil ratio (WOR) and oil recovery, respectively. The capillary pressure coefficient ratio between the matrix and the discrete fracture (B_m/B_i) varies from one to five. The results presented by Monteagudo and Firoozabadi (2004) are also shown in the figure.

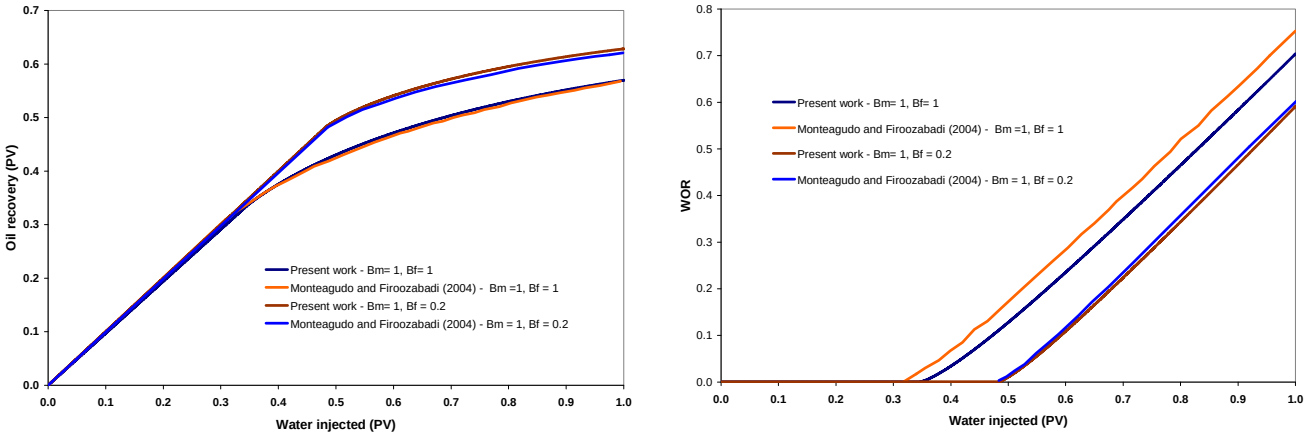

Figure 5. Case study 1. a) Oil recovery curves. b) Cumulative water and oil ratio curves.

From Figure 5, it is possible to observe that except for the WOR curve for $B_m = B_f = 1$, all the results are in good agreement with those presented by Monteagudo and Firoozabadi (2004). Several parameters such as the mesh size, maximum time step, and convergence criteria were changed, but the difference between the WOR curves for $B_f = B_m = 1$ of the present work and the one presented in the Montegudo and Firoozobadi (2004) did not decrease. However, it is important to mention that the difference between the water breakthrough was only about 0.029 PV (2.9 days). More importantly, the curves present almost the same trends. From Figure 5, it possible to verify that the capillary pressure ratio between the matrix and the discrete fracture has a strong effect in the oil recovery process. Increasing this ratio will delay the water breakthrough and increase the oil production. These phenomena were also observed by Monteagudo and Firoozabadi (2004).

Figure 6 presents water saturation field results for various values of B_m and B_f for case study 1. As shown in Fig. 5, there is a long delay in the water breakthrough when capillary pressure increases. This effect is clearly demonstrated in Fig. 6. The saturation fields shown in Figure 6 are similar to the ones presented by Monteagudo and Firoozabadi (2004).

Figure 7 presents the results for case study 2, in terms of the cumulative water and oil ratio (WOR) and oil recovery for matrix capillary pressure 0 and 1 as well as discrete fracture 0, 1, and 0.2. Again, we can see that capillary pressure has a strong effect in the oil recovery process.

Figure 8 presents the water saturation fields for the investigated parameters of case study 2 (see Fig. 7). When the saturation fields from Fig. 8 are compared to those presented in Fig 6, for case study 1, we observe that the main difference between the saturation fields is the large spread in the water saturation as shown in Figure 6. This spread in the water saturation fields is caused by the configuration discrete fractures.

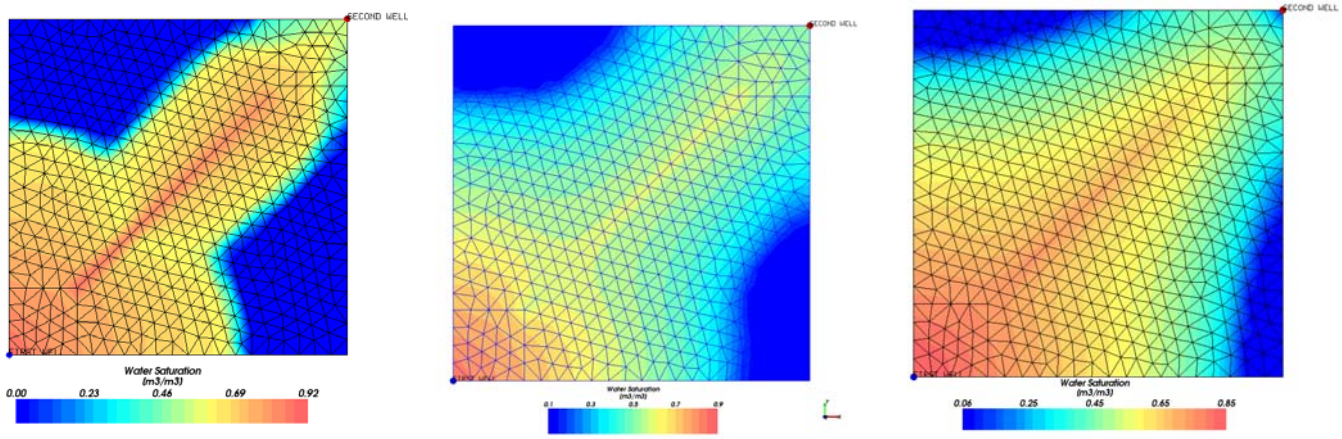

(a) (b) (c)

Figure 6. Water saturation fields for case study 1 at 0.5 PV (50 days). a) $B_m = B_f = 0$. b) $B_m = B_f = 1$. c) $B_m = 1$, $B_f = 0.2$.

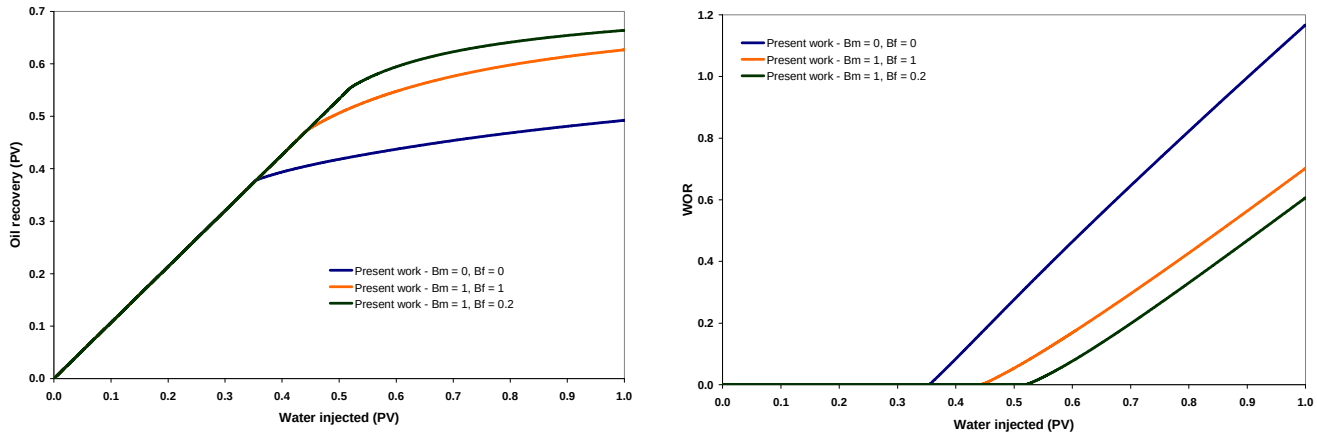

Figure 7. Case study 2. a) Oil recovery curves. b) Cumulative water and oil ratio curves.

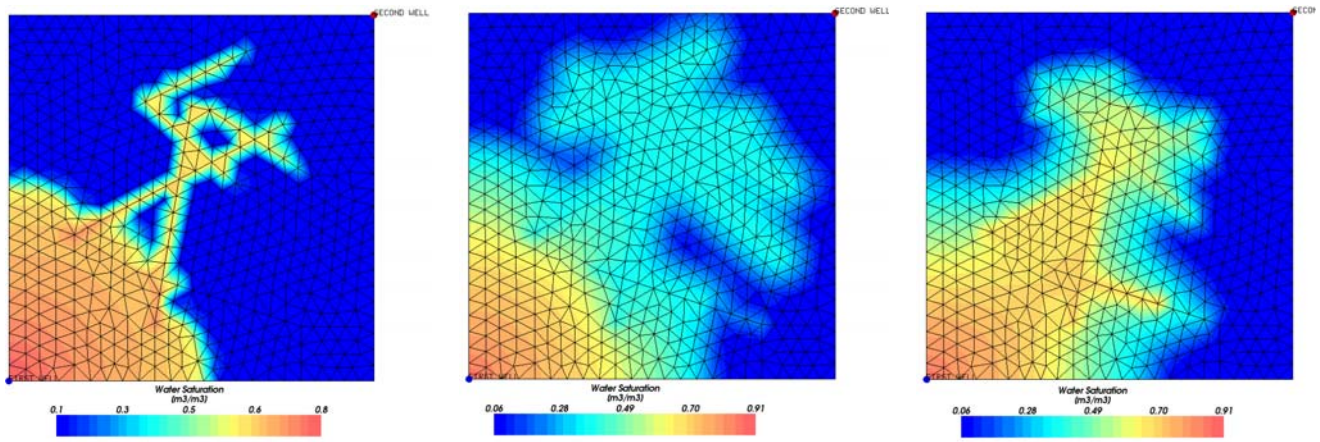

(a) (b) (c)

Figure 8. Water saturation fields for case study 2 at 0.25 PV (25 days). a) $B_m = B_f = 0$. b) $B_m = B_f = 1$. c) $B_m = 1$, $B_f = 0.2$.

Figure 9 presents the saturation fields for case study 3 at 0.146 PV (1000 days). Although the breakthrough did not occur in any producer well, it can be seen that the saturation front for the case with capillary pressure is delayed in comparison with the case without capillary pressure.

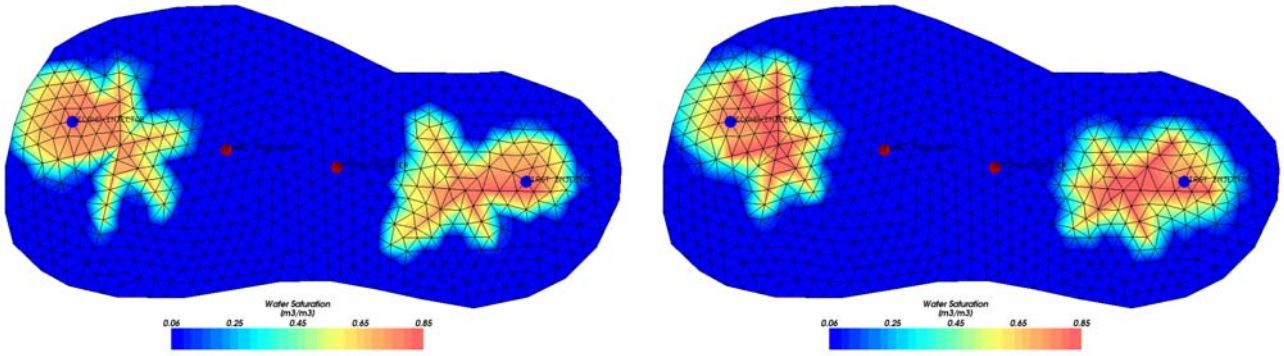

Figure 9. Water saturation fields for case study 3 at 0.146 PV (1000 days). a) $B_m = B_f = 0$. b) $B_m = 1$, $B_f = 0.2$.

6. Conclusions

We have presented an investigation of naturally-fractured reservoirs using the discrete fractured model in conjunction with an element-based finite-volume approach and unstructured grids. In the discrete fracture approach, both the discrete fracture and the matrix mass balances are taken into account without any additional formulations to couple the matrix and discrete fractures. For the 2D reservoirs shown in this paper, the discrete fracture model is 1D and the discrete fractures are located along the edges of each element. Capillary pressure was included in both matrix and discrete fracture media. We have shown the results for several discrete fractures configurations. The presented results were in good agreement with similar approach described in the literature. In order to be more realistic from a compositional reservoir modeling point of view, the discrete fracture model is being implemented to include the gas phase. Also, the implementation of this model for 3D reservoirs is underway.

7. Acknowledgments

This work was conducted with the support of the Reservoir Simulation Joint Industry Project, a consortium of operating and service companies at the Center for Petroleum and Geosystems Engineering at The University of Texas at Austin. The authors would like to thank The Engineering Simulation Scientific Software (ESSS) for giving us the KRAKEN pre-processing and processing software. Also, the first author would like to thank CNPq (The National Council for Scientific and Technological Development of Brazil) for their financial support.

8. References

Al-Huthali, A. H. and Datta-Gupta, A., 2004, Streamline Simulation of Water Injection in Naturally Fractured Reservoirs, The SPE/DOE Fourteenth Symposium on Improved Oil Recovery, Tulsa, Oklahoma, 17–21 April.

Baca, R. G., Arnett, R. C., and Langford, D. W., 2005, Modelling Fluid Flow in Fractured-Porous Rock Masses by Finite-Element Techniques, International Journal for Numerical Methods in Fluids, 4(4), pp. 337–348.

Cordazzo, J., 2004, An Element Based Conservative Scheme Using Unstructured Grids for Reservoir Simulation, SPE International Student Paper Contest, The SPE Annual Technical Conference and Exhibition, Houston, Texas.

Cordazzo, J., Maliska, C. R., Silva, A. F. C., and Hurtado, F. S. V., 2004, The Negative Transmissibility Issue When Using CVFEM in Petroleum Reservoir Simulation - 1. Theory, Braz. Soc. of Mechanical Sciences and Engineering - ABCM, Rio de Janeiro, Brazil, Nov. 29–Dec. 03.

Cordazzo, J., Maliska, C. R., Silva, A. F. C., and Hurtado, F. S. V., 2004, The Negative Transmissibility Issue When Using CVFEM in Petroleum Reservoir Simulation - 2. Results, Braz. Soc. of Mechanical Sciences and Engineering - ABCM, Rio de Janeiro, Brazil, Nov. 29–Dec. 03.

Kazemi, H., 1969, Pressure Transient Analysis of Naturally Fractured Reservoirs, SPE Journal, pp. 451–462, December.

Kazemi, H., Merrill Jr., L. S., Porterfield, K. L., and Zeman, P. R., 1976, Numerical Simulation of Water-Oil Flow in Naturally Fractured Reservoirs, December.

Karpinsk, L., Maliska, C.R., Marcondes, F. Delshad, M., and Sepehrnoori, K., 2009, An Element Based Conservative Approach Using Unstructured Grids in Conjunction with a Chemical Flooding Compositional Reservoir Simulator, 20th International Congress of Mechanical Engineering, Gramado, RS.

Lingen, P., Sengul, M., and Daniel, J.-M., 2001, Single Medium Simulation of Reservoirs with Conductive Faults and Fractures, the 2001 SPE Middle East Oil, Bahrain.

Magras, J-F., Quandalle, P., and Beicip-Franlab. P. B., 2001, High-Performance Reservoir Simulation with Parallel ATHOS, SPE Reservoir Simulation Symposium, Houston, Texas, 11–14 February.

Maliska, C. R., 2004, Heat Transfer and Computational Fluid Mechanics, Florianópolis, 2ª. Ed. Editora LTC. (In Portuguese).

Marcondes, F. and Sepehrnoori, K., 2007, Unstructured Grids and an Element Based Conservative Approach for Compositional Reservoir Simulation, The 19th International Congress of Mechanical Engineering, November 5–9, Brasília, DF, Brazil.

Marcondes, F. and Sepehrnoori, K., 2010, An Element-Based Finite-Volume Method Approach for Heterogeneous and Anisotropic Compositional Reservoir Simulation, Journal of Petroleum Science and Engineering, 73, pp. 99–106.

Monteagudo, J. E. P. and Firoozabadi, A., 2004, Control-Volume Method for Numerical Simulation of Two-Phase Immiscible Flow in Two- and Three-Dimensional Discrete Fractured Media, Water Reseources, 40, pp. 1–20.

Naimi-Tajdar, R., Han, C., Sepehrnoori, K., Arbogast, T. J., and Miller, M. M., 2007, A Fully Implicit, Compositional, Parallel Simulator for IOR Processes in Fractured Reservoirs, SPE Journal, pp. 367–381.

Noorishad, J. and Mehran, M., 1982, An Upstream Finite Element Method for Solution of Transient Transport Equation in Fractured Porous Media, Water Resources Research, 18(3), pp. 588–596.

Odeh, A. S., 1965, Unsteady-State Behavior of Naturally Fractured Reservoirs, SPE Journal, Trans. AIME, 234, pp. 60–66, March.

Parashar, M., Wheeler, J. A., Pope, G., Wang, K., and Wang, P., 1997, A New Generation EOS Compositional Reservoir Simulator: Part II – Framework and Multiprocessing, Paper SPE 37977, SPE Reservoir Simulation Symposium, Dallas, USA.

von Pattay, P. W. and Ganzer, L. J., 2001, Reservoir Simulation Model for Fractured and Partially Fractured Reservoirs Based on PEBI Grids, SPE Reservoir Simulation Symposium, Houston, Texas, 11–14 February.

Wang, P., Yotov, I., Wheeler, M., Arbogast, T., Dawson, C., Parashar, M., and Sepehrnoori, K., 1997, A New Generation EOS Compositional Reservoir Simulator: Part I – Formulation and Discretization, Paper SPE 37079, SPE Reservoir Simulation Symposium, Dallas, Texas.

Warren, J. E. and Root, P. J., 1963, The Behavior of Naturally Fractured Reservoirs, SPE Journal, pp. 245–255, September.

7. RESPONSIBILITY NOTICE

The authors are the only ones responsible for the printed material included in this paper.